JOURNAL OF CATALYSIS **164,** 173–183 (1996)
ARTICLE NO. 0373

Modification of the Redox Behaviour of CeO_2 Induced by Structural Doping with ZrO_2

P. Fornasiero,* G. Balducci,* R. Di Monte,* J. Kašpar,*,[1] V. Sergo,† G. Gubitosa,‡ A. Ferrero,‡ and M. Graziani*

*Dipartimento di Scienze Chimiche, Università di Trieste, Via Giorgieri 1, 34127 Trieste, Italy; †Dipartimento di Ingegneria dei Materiali e Chimica Applicata, Università di Trieste, Via A. Valerio 2, 34127 Trieste, Italy; and ‡Magneti Marelli D.S.S., Viale Carlo Emanuele II 150, 10078 Venaria Reale (TO), Italy

Received January 19, 1996; revised April 10, 1996; accepted May 31, 1996

Reduction/oxidation behaviour of high surface area CeO_2 and $Ce_{0.5}Zr_{0.5}O_2$ mixed oxide is compared. It is shown that introduction of ZrO_2 into the CeO_2 framework with formation of a solid solution strongly modifies the reduction behaviour in comparison to that seen with CeO_2 alone. Remarkably, upon repetitive reduction/oxidation processes, the temperature of the reduction of the solid solution decreases from 900 to 700 K. Conversely, in the aged CeO_2 sample almost no reduction occurs below 900 K. Textural characterisation shows that the redox process favours a large sintering of both the samples and, unexpectedly, induces formation of a new mesoporosity centered at about 20 nm. The expansion/contraction of the lattice parameter upon, respectively, reduction/oxidation, detected by X-ray diffraction, is suggested to be responsible for the textural modification. The suppression of the redox capacities of CeO_2 at moderate temperature is associated with the decrease of the surface area. The sintering process induces a structural modification of $Ce_{0.5}Zr_{0.5}O_2$ which promotes the reduction in the bulk, resulting in a high efficiency of the $Ce^{4+} \rightleftharpoons Ce^{3+}$ redox cycle at moderate temperatures.

INTRODUCTION

The oxygen storage capacity (OSC) of CeO_2 due to its ability to undergo rapid reduction/oxidation cycles, according to the reaction $2CeO_2 \rightleftharpoons Ce_2O_3 + 1/2O_2$, is of relevant technological importance in automotive exhaust catalysis. The highest simultaneous conversions of the three pollutants CO, hydrocarbons (HC), and NO_x are indeed attained over a three-way catalyst (TWC) at air/fuel (A/F) ratios close to the stoichiometric value. Excursions to fuel-lean (net oxidizing) and fuel-rich (net reducing) conditions severely decrease, respectively, NO and CO HC conversions. The OSC of added CeO_2 acts as an oxygen partial pressure regulator, minimising these undesirable effects (1).

In pure CeO_2, the Ce^{3+}/Ce^{4+} redox process is essentially limited to the surface up to 620–670 K (2, 3). It is desirable for the TWCs to be effective at temperatures as low as possible and therefore, high surface area is an essential prerequisite in obtaining good efficiency of the Ce^{3+}/Ce^{4+} redox cycle, i.e., high OSC. The redox behaviour of CeO_2 strongly depends on textural properties because a decrease of surface area depresses all the surface related redox processes (2). Of the two processes concerned with the OSC, the oxidation is facile and it occurs at room temperature (rt) (4, 5), while the reduction of ceria starts at about 473 K and is essentially limited to the uppermost layer of the oxide up to 620–670 K (2).

Above 623 K, the CeO_2 surface is unstable in the presence of H_2 and collapse of surface area, due to pore filling, occurs concurrently with its reduction (5).

High thermal stability is an essential requirement for the CeO_2-containing supports since a close coupled location of the converter is often employed in automotive applications and the TWCs can meet temperatures up to 1200 K.

As a part of our studies on the applications of CeO_2–ZrO_2 mixed oxides as supports for noble metal catalysts for the reduction of NO by CO, we previously investigated the reduction/oxidation behaviour of a series of Rh-loaded $Ce_xZr_{1-x}O_2$ ($x = 0.1$–1) mixed oxides and found that incorporation of ZrO_2 into a solid solution with CeO_2 strongly favours the reduction of the support (6). We observed that the reduction behaviour strongly depends both on the content of ZrO_2 in the solid solution and on the nature of the phase present. The mixed oxide supports were prepared by the usual practice of firing a mechanically ground mixture of the oxide precursors at 1873 K. Such a procedure ensures formation of a solid solution, but the product is very dense, lacking the high surface area and pore volume desired for catalytic applications (7). In the present work, the reduction/oxidation behaviour of a CeO_2–ZrO_2 sample with a surface area of 64 $m^2\ g^{-1}$ is therefore investigated. The aim was to verify the influence of the initial texture of the solid

[1] To whom correspondence should be addressed.

0021-9517/96 $18.00

solution on the redox processes. The results are compared with those of high surface area CeO_2 (196 $m^2\ g^{-1}$) to elucidate the role of ZrO_2 in promoting the OSC. A preliminary report of this work has recently appeared (8).

EXPERIMENTAL

The low surface area ($\approx$1 $m^2\ g^{-1}$) solid $Ce_{0.5}Zr_{0.5}O_2$ solution was that from a previous study (6). The high surface area sample was prepared by a homogeneous gel route from $Ce(acac)_4$ and $Zr(O\text{-}Bu)_4$ precursors (Aldrich) according to a previous report (9). The sample was calcined at 773 K in air for 5 h. Henceforth, this sample is indicated as fresh $Ce_{0.5}Zr_{0.5}O_2$. High surface area CeO_2 (196 $m^2\ g^{-1}$) was kindly provided by Dr. L. Murrel.

Powder X-ray diffraction (XRD) patterns were collected on a Siemens Kristalloflex Mod.F Instrument (Ni-filtered Cu$K\alpha$). Cell parameters were determined by using the TREOR90 program which employs the Visser algorithm. The peak deconvolution was carried out after the subtraction of contribution of the K_{α_2} line to the spectrum. Pearson VII functions were employed for the peak deconvolution. In order to minimise the reoxidation of the reduced samples during the XRD measurements, care was taken to limit the exposure to air. Separate O_2 uptake measurements showed that less then 8% of Ce^{3+} present in the reduced samples is oxidized at rt. FT-Raman spectra were obtained on a Perkin Elmer 2000 FT-Raman spectrometer with a diode pumped YAG laser and a rt super InGaAs detector. The laser power was 50–200 mW. Scanning electron microscopy (SEM) was carried out on a JEOL 300 microscope using an accelerating voltage of 20 kV. Samples of the catalysts were deposited on the holder and successively gold or copper coated (3 nm) in order to reduce the charge buildup on the sample. N_2 adsorption isotherms at 77 K were obtained on a Micromeritics ASAP 2000 analyzer.

Temperature programmed reduction (TPR) experiments were carried out either in a conventional system equipped with a thermal conductivity detector or in a TG-DTA apparatus. Before the initial TPR experiment, all the samples were pretreated in Ar (20 ml min^{-1}) at 900 K for 5 h. Neither CO_2 evolution nor appreciable O_2 uptake could be detected after such thermal treatment using a quadrupole mass analyzer and the TPR/O_2 pulse uptake equipment, respectively. The reduction was carried out in a flow of H_2 (5%) in Ar (25 ml min^{-1}) using a heating rate of 10 K min^{-1} in the former equipment and 2 K min^{-1} in the latter. Typically, the reduction was carried out up to 1273 K and then the sample (0.04–0.07 g) was held at this temperature for 30 min. In such operating condtions unperturbed reduction profiles are obtained since interferences due to mass transfer limitations or dispersion effects are minimised (10). The amount of H_2 uptake in the TPR was estimated from integrated peak areas by comparision with those obtained by using CuO as a standard. The reproducibility of the method was periodically checked and a standard deviation for the overall H_2 uptake of $\pm$1.0 ml g^{-1} was measured. Oxygen uptake was measured by pulse technique after the reduction. H_2 was desorbed at $T \geq 700$ K in Ar flow (30 min, 20 ml min^{-1}) before the measurement. The oxygen uptake was then measured at 700 K by injecting pulses of O_2 (0.092 ml) into the flow of Ar passing over the catalyst until the breakthrough point was attained.

RESULTS AND DISCUSSION

Before presenting and discussing the results in detail, it is useful to recall the essential features of the CeO_2–ZrO_2 system. Below 1273 K, the phase diagram shows a monophase region of monoclinic (*m*) symmetry for CeO_2 molar contents of less than 20%, while for CeO_2 contents higher than 80% cubic (*c*) phase was reported (11, 12). In the intermediate region, the true nature of the CeO_2–ZrO_2 phase diagram is still matter of debate (13) due to the presence of a number of stable and metastable phases of tetragonal symmetry (11–14). According to recent investigations, three different *t*, *t′*, and *t″* phases can be distiguished on the basis of XRD and Raman characterisation (13, 15, 16). Of these, the *t* form is a stable one formed through a diffusional phase decomposition, the *t′* form is obtained through a diffusionless transition and it is metastable, and the *t″* form is intermediate between *t′* and *c*. It shows no tetragonality and it exhibits an oxygen displacement from ideal fluorite sites (15, 16). The *t″* phase is generally referred to as a *cubic* phase because its XRD pattern is indexed in the cubic Fm3m space group. This is due to the fact that the XRD pattern is generated essentially by the cation sublattice. Consistently, in the following we will apply the term *cubic* to both the *c* and the *t″* phases. For sake of clarity the characteristics of all the phases are summarised in Table 1.

TABLE 1

Classification of the Phases in the CeO_2–ZrO_2 Binary System[a]

Phase	Composition range (% mol Ce)	Tetragonality[b]	Space group
Monoclinic (*m*)	0–20	—	$P2_1/c$
Tetragonal (*t*)	20–40	>1	$P4_2/nmc$
Tetragonal (*t′*)	40–65	>1	$P4_2/nmc$
Tetragonal (*t″*)[c]	65–80	1	$P4_2/nmc$
Cubic (*c*)	80–100	1	Fm3m

[a] The classification reported here follows that proposed in Refs. 15 and 16. The *t* and *t′* phases correspond to the TZ° and TZ′ phases previously reported by Meriani *et al.* (14, 17).

[b] Defined as axial ratio *c*/*a*.

[c] As explained in the text, on the basis of the XRD pattern this phase is commonly indexed in the Fm3m space group (14, 17).

As previously reported (6), the *cubic* $Rh/Ce_{0.5}Zr_{0.5}O_2$ showed the best ability to undergo reduction in the bulk of the solid solutions which occurred at a temperature as low as 600 K.This was attributed to the fact that this composition presents the highest ZrO_2 content compatible with the *cubic* symmetry. We have decided to investigate the effects of the texture on the redox behaviour of $Ce_{0.5}Zr_{0.5}O_2$. This composition represents a further point of interest since it is located at the limit of the *cubic–t′* transition which allows one to prepare either tetragonal or *cubic* form by simply changing the preparation conditions (13).

Characterisation of the Fresh $Ce_{0.5}Zr_{0.5}O_2$

The powder X-ray pattern of the fresh $Ce_{0.5}Zr_{0.5}O_2$ is reported in Fig. 1 (trace 1). It features broad peaks attributed to the presence of small crystallites which are formed after the calcination at 773 K. An estimate of the average particle size by the line broadening method gives a value of 5.4 nm. The width of the XRD peaks does not allow one to assign the reported pattern to a *cubic* phase unequivocally since the presence of the *t′* phase is usually detected by broadening and splitting of the peaks observed in CeO_2 at about 47° and 59° (2θ) which are indexed, respectively, as (220) and (222) planes in the Fm3m space group (17).

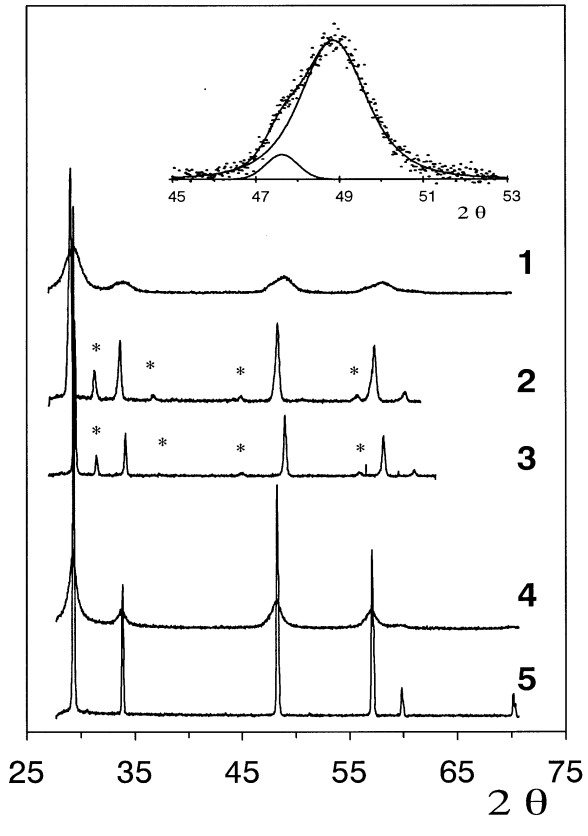

FIG. 1. Powder XRD patterns of (1) fresh, (2) reduced at 1273 K, and (3) oxidized $Ce_{0.5}Zr_{0.5}O_2$ and (4) fresh and (5) reduced/oxidized CeO_2. In the inset the fitted and experimental profiles of the peak at 49° 2θ of trace 1 are compared. For peaks indicated with an asterisk, see text.

Deconvolution of the experimental XRD pattern for the peak at 49° (2θ) is reported in the inset of Fig. 1. It appears clearly that the width and asymmetry of the peak is best attributed to a contribution of two peaks centered at 47.3° and 49.0° (2θ). The former is due to the presence of an almost pure CeO_2 phase. This suggests that during the synthesis a small part of the cerium (about 8%) was not incorporated. The above reported result of the deconvolution further supports the attribution of the XRD pattern to a *cubic* phase, since tetragonalization of the unit cell ($c/a > 1$) would be detected by splitting of the peak at 49° (2θ) at the high 2θ tail. As shown below, the attribution to a *cubic* phase is also supported by Raman spectra. The refinement of the XRD pattern shown in the trace 1 of Fig. 1 gives a lattice parameter of 5.265(5) Å which compares well with the of 5.274(1) Å measured in a highly crystalline *cubic* $Ce_{0.5}Zr_{0.5}O_2$ sample prepared from the oxides by a high temperature solid state reaction and quenched to rt (13).

The Raman spectrum of the $Ce_{0.5}Zr_{0.5}O_2$ calcined at 773 K is reported in spectrum 1 of Fig. 2. It features a strong broad band centered at 465 cm^{-1} with a shoulder at about 550 cm^{-1} and two bands at 313 (w) and 140 (vw) cm^{-1}. Six Raman-active modes of $A_{1g} + 3E_g + 2B_{1g}$ symmetry are observed for tetragonal ZrO_2 (space group $P4_2/nmc$), while for the cubic fluorite structure (space group Fm3m) only one F_{2g} mode centered at around 490 cm^{-1} is Raman-active (13, 18). In the pure CeO_2, which also has the fluorite structure, the F_{2g} mode is observed 465 cm^{-1}. The peak at 465 cm^{-1} is therefore consistent with the presence of a *cubic* phase. A high frequency tail of the Raman mode at 465 cm^{-1} was observed in CeO_2-trivalent rare earth mixed oxides and was associated with the oxygen vacancies created upon Ce^{4+} substitution (19). The presence of a substantial amount of defects in the CeO_2–ZrO_2 mixed oxides was revealed by density measurements (6, 20) even though their exact nature could not yet be ascertained (6). The attribution of the bands at 313 and 140 cm^{-1} to the *t* or *t′* phase can be ruled out on the basis of the following observation: in the pure tetragonal ZrO_2, two strong absorption bands were observed at 263 and 148 cm^{-1} whose frequencies, however, shift towards lower values in the tetragonal *t*-$Ce_{0.12}Zr_{0.88}O_2$ mixed oxide (21).

In a recent investigation of the CeO_2–ZrO_2 system (15), the appearance of a strong band at approximately 460 cm^{-1} and weak bands at 150, 180, 300 cm^{-1} was observed for a $Ce_{0.7}Zr_{0.3}O_2$ sample and it was attributed to the formation the *t″* phase. Spectrum 1 in Fig. 2 closely resembles that reported in Ref. 15 suggesting that the *t′*–*t″* phase boundary can shift to CeO_2 contents lower than 70%.

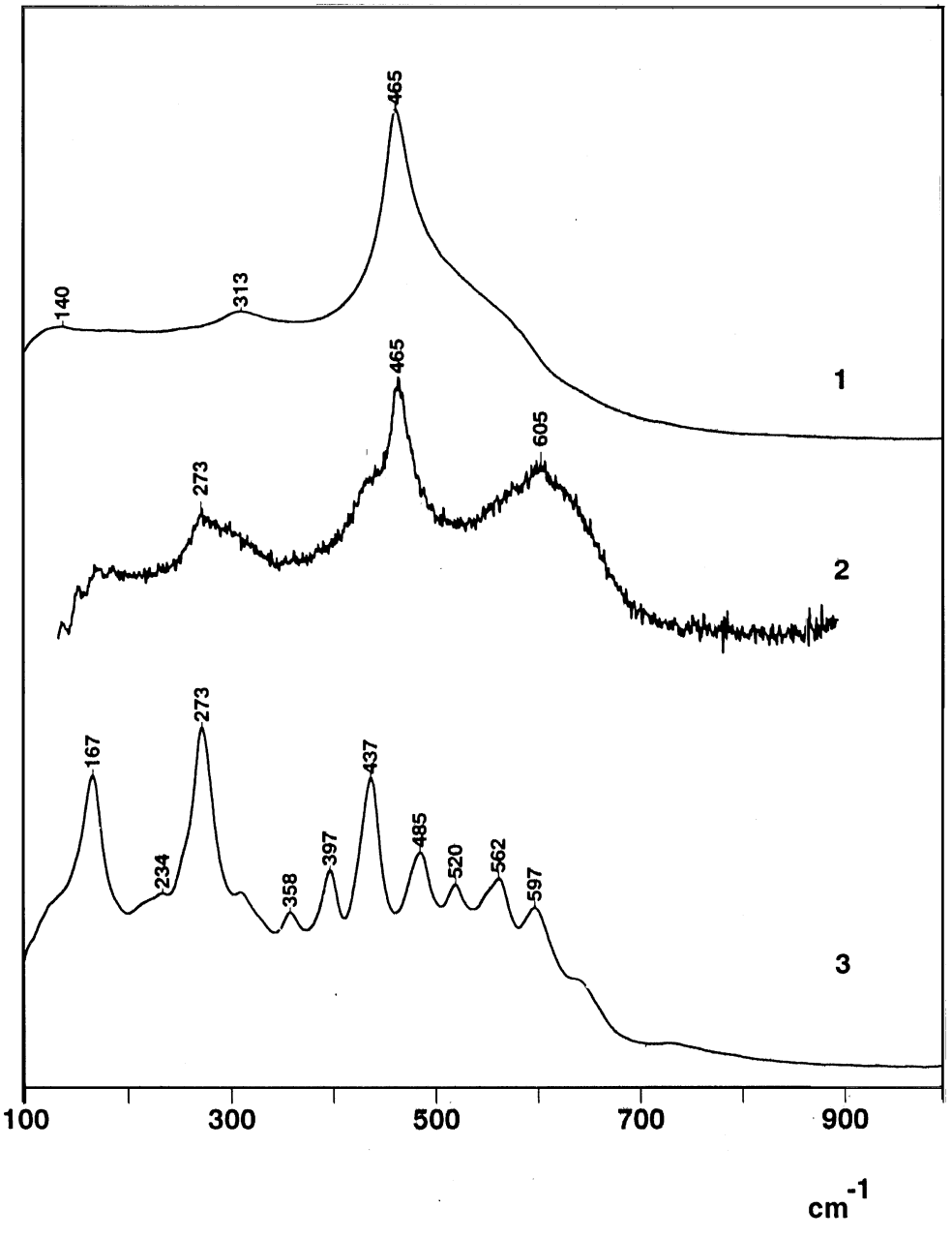

FIG. 2. Raman spectra of $Ce_{0.5}Zr_{0.5}O_2$: (1) fresh, (2) reduced at 1000 K and oxidized at 700 K, (3) reduced at 1273 K and oxidized at 700 K for three times. All the spectra are displaced vertically and trace 2 is expanded.

The formation of the thermodynamically unfavoured tetragonal phase during the synthesis of ZrO_2 has often been observed and different explanations have been advanced to account for the stabilisation of *t*-ZrO_2: surface and strain energy effects (22), strain energy effects generated at domain boundaries (23), structural similarity (24), and/or topotactic crystallisation (25) of *t*-ZrO_2 from the amorphous phase. The latter two explanations are rather more kinetic than thermodynamic. Nevertheless, all these investigations indicate that below a critical crystallite size, the tetragonal phase is favoured over the monoclinic one. Consistently, by using extremely fine particles, even the *c*-ZrO_2 was stabilised at rt (26). The presence of the *t″* form in the $Ce_{0.5}Zr_{0.5}O_2$ sample can therefore be attributed to the formation of small crystallites in the synthesis from the gel precursor. Formation of a *cubic* phase which is stable even after calcination at 773 K at such low content of CeO_2 is significant in view of the previous finding that low CeO_2 contents and *cubic* phase favour high OSC (6). The critical importance of the particle size in the phase stabilisation is

confirmed by the observation that, after calcination in air above 1073 K, tetragonalization of the sample to give a t'-$Ce_{0.5}Zr_{0.5}O_2$ phase is observed. Concurrently, particle size strongly increases as indicated by XRD.

Reduction–Oxidation Behaviour of $Ce_{0.5}Zr_{0.5}O_2$ and CeO_2

The reduction behaviour of $Ce_{0.5}Zr_{0.5}O_2$ and CeO_2 was investigated by means of the TPR technique. In order to eliminate the contribution of surface carbonates (4, 27), all the samples were thermally pretreated (see Experimental).

The TPR profile of the fresh $Ce_{0.5}Zr_{0.5}O_2$ and the effects of subsequent reoxidation and reduction cycles are compared in Fig. 3 with those of pure CeO_2. Two peaks, at 880 and 1010 K, respectively, are observed for the fresh solid solution. For comparison, low surface area $Ce_{0.5}Zr_{0.5}O_2$ (≈ 1 m^2 g^{-1}) does not show appreciable reduction below 1000 K (Fig. 3, trace 5).

After reoxidation at 700 K, these peaks disappear and new features at *lower* temperatures (695, 850 K) are observed in the second TPR experiment. Upon further recycling through repetitive reduction/oxidation cycles, the TPR profile still changes to reach the final aspect shown in trace 4 of Fig. 3, which features two broad peaks centered at 690–695 and 845 K. The reduction is complete by 950 K.

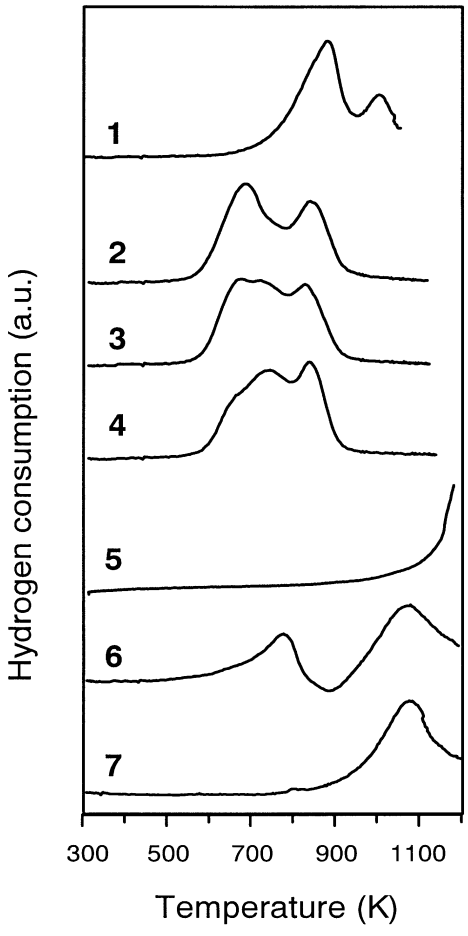

FIG. 3. TPR profile of (1) fresh $Ce_{0.5}Zr_{0.5}O_2$ and (2–4) recycled, respectively, 1, 4, and 7 times; (5) sintered (≈ 1 m^2 g^{-1}) $Ce_{0.5}Zr_{0.5}O_2$; (6) fresh CeO_2 and (7) recycled 2 times.

The comparison with the TPR profiles of CeO_2 is significant (Fig. 3, traces 6–7). Fresh CeO_2 features two reduction peaks at 790 and 1100 K. Reduction of CeO_2 has been thoroughly investigated and most of the previous investigations agree on attribution of these peaks to surface and bulk reduction, respectively (3), although the formation of nonstoichiometric CeO_{2-x} phases (4) and/or formation of hydrogen bronzes (28) in correspondence with the former peak, cannot be excluded. After reoxidation at 700 K, the subsequent TPR featured the profile reported in trace 7 of Fig. 3 with almost no reduction below 900 K due to collapse of the surface area. Repetitive reoxidation/reduction cycles did not modify this profile further.

The onset of H_2 consumption at about 800 K observed in the recycled CeO_2 samples is higher when compared with the previous observation that the reduction of CeO_2 starts at about 473 K (4). In the TPR experiment, the reduction process is kinetically rather than thermodynamically controlled, resulting in a net shift of the reduction temperature toward higher values with respect to isothermal reduction.

The attribution of the reduction peaks in the case of $Ce_{0.5}Zr_{0.5}O_2$ is not straightforward. The width and the overlapping of the reduction peaks does not allow one to evaluate directly the relative amounts of H_2 consumed in the course of the TPR. However, as recently suggested for reduction of CeO_2 samples with different textures, the contribution of the surface reduction can be evaluated by considering symmetrical reduction profiles (2). This observation is further supported by a recent analysis of the shapes of the TPR profiles reported by Fierro *et al.* (29), who showed that the peak profile can be confidently described by Gaussian type profiles. The reduction profiles reported in Fig. 3 for the $Ce_{0.5}Zr_{0.5}O_2$ sample were successfully deconvoluted into three Gaussians and the relative H_2 consumptions calculated.

Some representative results of the peak deconvolution are reported in Table 2. The comparison of the experimental and fitted reduction profiles reported in Fig. 4 clearly shows that this procedure allows one to obtain a reasonable fit of the experimental TPR profile. A perusal of the data reported in Table 2 reveals that all the TPR profiles can be successfully described as the sum of three processes. Except for the fresh sample, all the reduction processes peak at approximately 665–675, 740–760, and 840–860 K. The modification of the TPR profiles of the recycled samples reported in Fig. 3 should be ascribed essentially to a variation of the relative intensities of the peaks described by the Gaussian functions while both the overall H_2 consumption and the peak temperatures are almost constant.

TABLE 2

Calculated H_2 Consumption and Peak Temperatures in the Temperature Programmed Reduction of Fresh and Recycled $Ce_{0.5}Zr_{0.5}O_2$

No. of recycles	Peak temperatures (K)			H_2 consumption[a] ($ml\ g^{-1}$)		
0	830	885	1010	10	6	9
1	675	756	858	8	14	5
4	664	745	839	3	16	7
7	674	743	857	1	18	7

[a] Hydrogen consumption calculated for the first, second, and third peak, respectively (see text).

TABLE 3

H_2 Consumption and O_2 Uptakes Measured in the TPR/Oxidation Experiments Carried out on $Ce_{0.5}Zr_{0.5}O_2$ and CeO_2

Sample	No. of recycles	H_2 consumption[a] ($ml\ g^{-1}$)	O_2 uptake ($ml\ g^{-1}$)	Ce^{3+} (%)[b]
$Ce_{0.5}Zr_{0.5}O_2$	0	25	11.8	62
	1	27	11.3	59
	2–7	26	10.3	54
	8	23[c]	9.9	52
	9	13[d]	7.2	38
CeO_2	0	22	11.3	35
	1–3	20	11.3	35
	4	1[c]	0.4	1

[a] Standard deviation ±1–2 $ml\ g^{-1}$.
[b] Estimated from O_2 uptake.
[c] Reduced at 700 K for 2 h.
[d] Reduced at 600 K for 2 h.

It is generally accepted that the low temperature process accounts for reduction of the surface. The progressive decrease of the amount of H_2 consumed in the first peak in the case of $Ce_{0.5}Zr_{0.5}O_2$ upon cycling the sample through the redox process strongly suggests that this peak should be associated with the surface reduction. On this assumption, a surface area of 10 $m^2\ g^{-1}$ can be estimated according to Ref. 2 for the sevenfold recycled sample which is quite close to that obtained after an isothermal reduction at 1000 K (Table 4).

The two peaks at 740–760 and 840–860 K are therefore attributed to reduction processes occurring in the bulk of the solid solution. The presence of two peaks for bulk reduction was previously reported (6) and it was attributed to clustering of bulk oxygen vacancies (30).

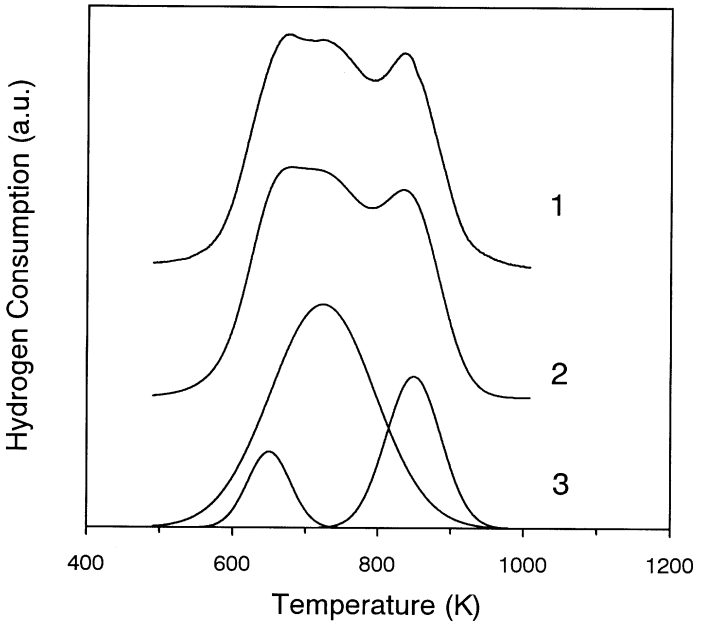

FIG. 4. Comparison of TPR profiles of threefold recycled $Ce_{0.5}Zr_{0.5}O_2$. (1) Experimental and (2) fitted patterns; (3) the three Gaussians employed for the fitted pattern.

As far as the TPR profile of the fresh $Ce_{0.5}Zr_{0.5}O_2$ is concerned, it should be noted that the amount of H_2 consumed for the first reduction peak is far higher than that estimated for the surface reduction, suggesting that reduction at the surface and in the bulk occurs concurrently.

Another point worth noting is that the reduction of the fresh sample starts at a temperature which is about 100 K higher than in the recycled samples. For CeO_2 surface, H_2 dissociation with formation of supplementary OH groups was observed above 473 K, (2, 4), while dissociation of H_2 occurred over degassed ZrO_2 surfaces already at rt (31). The higher ionic character of the Zr–O bond compared to the Ce–O bond promotes the hydrophilicity of the ZrO_2 surface, making the surface rehydroxylation an easy process (32). Upon thermal treatment the ZrO_2 surface shows a depletion of oxygen at the surface which is an indication of Lewis type acidity (33). Accordingly, we suggest that on increasing the temperature during the TPR experiment, progressive elimination of surface OH groups will occur which could generate surface sites of strong Lewis acidity. Such sites may play a role in H_2 activation, accounting for the lower temperature of surface reduction upon recycling of the $Ce_{0.5}Zr_{0.5}O_2$. On the other hand, during the TPR of the fresh sample, collapse of surface area and pore filling occur which hinders the concomitant reduction process.

An extremely limited amount of surface OH groups can account for the lack of reduction of the low surface area $Ce_{0.5}Zr_{0.5}O_2$ below 1000 K. It must be recalled that this sample was prepared by calcination at 1873 K (6). This confirms the importance of the initial texture on the redox properties.

The oxygen uptakes were measured both after the reduction of the fresh and recycled samples (Table 3). The degree of reduction of CeO_2 at 1273 K is independent of the sample history. The amount of oxygen vacancies calculated from the O_2 uptake after the reduction at 1273 K of fresh CeO_2 gives a final composition of $CeO_{1.83}$.

TABLE 4

Textural Modifications of CeO_2 and $Ce_{0.5}Zr_{0.5}O_2$ Induced by *in Situ* Thermal, H_2, and O_2 Treatments[a]

Sample	Treatment[b]			BET surface area ($m^2\ g^{-1}$)	Pore volume ($ml\ g^{-1}$)[c]			
						Mesopore	Micropore	
	T (K)	Gas	Time (h)		Total	V_{BJH}	V_t	V_{DR}
CeO_2				196	0.15	0.08	0.08	0.08
	900	N_2	5	155				
	623	H_2	2	158				
	700	O_2	0.5	153				
	780	H_2	2	115				
	700	O_2	0.5	117				
	900	H_2	2	30				
	700	O_2	0.5	32				
	1000	H_2	2	11				
	700	O_2	0.5	12	0.04	0.04	—	—
$Ce_{0.5}Zr_{0.5}O_2$				64	0.06	0.04	0.03	0.025
	900	N_2	5	42				
	780	H_2	2	28				
	700	O_2	0.5					
	900	H_2	2	13				
	700	O_2	0.5					
	1000	H_2	2	9.5				
	700	O_2	0.5	12	0.06	0.06	—	—

[a] All the samples were degassed at 623 K prior to N_2 adsorption.
[b] Treatment in flow of N_2 (20 ml min^{-1}), H_2 (20 ml min^{-1}), or O_2 (20 ml min^{-1}).
[c] Values determined from the adsorption isotherm by using the BHJ method in the range 3.5–170 nm, the t plot and the Dubinin Radushkevich plot in the range 2×10^{-5}–0.1 p/p_0, and total pore volume calculated at $p/p_0 = 0.98$ (35).

Consistently with the TPR profiles, the reduction of the CeO_2 up to 1273 K strongly depresses the ability to adsorb oxygen after a low temperature reduction. This ability is present only in the fresh sample reduced at 700 K and it is retained until CeO_2 is reduced at a high temperature.

For $Ce_{0.5}Zr_{0.5}O_2$, a small decrease of the oxygen uptake is observed during the first two runs, but after the second recycle a constant oxygen uptake is observed in all the subsequent experiments (Table 3). The redox process in $Ce_{0.5}Zr_{0.5}O_2$ is more efficient than in CeO_2 since more cerium (50–60%) is reduced at 700–1273 K. A final composition of $Ce_{0.5}Zr_{0.5}O_{1.84}$ is estimated after the reduction of the fresh sample at 1273 K. An important finding of the present work is that, at variance with CeO_2, the recycled $Ce_{0.5}Zr_{0.5}O_2$ is able to adsorb oxygen after a low temperature reduction.

Modification of the Textural and Structural Properties Induced by the Redox Cycles

N_2 physisorption at 77 K. The influence of the thermal treatments on the textural properties was investigated by means of N_2 physisorption at 77 K. The results are reported in Table 4 and Fig. 5, respectively. Both fresh $Ce_{0.5}Zr_{0.5}O_2$ and CeO_2 show an isotherm of type IV and H2 hysteresis according to the IUPAC classification (34) which are indicative of the presence of a mesoporous texture with a substantial contribution from micropores in the case of CeO_2. Consistently, we found a high value of the BET constant $c = 250$ (35). From the adsorbed volume vs t plot, a micropore area of 34 $m^2\ g^{-1}$ is calculated according to Harkins and Jura (36). The t plot (not reported) is linear in the range 0.35–0.5 nm and shows a downward deviation from the linearity for $t > 0.5$ nm confirming the presence of micropores (37).

After a thermal treatment in N_2 at 900 K, surface area decreases by 20 and 35% for CeO_2 and the $Ce_{0.5}Zr_{0.5}O_2$ sample, respectively. The micropore area of the CeO_2 decreases from 34 to 10 $m^2\ g^{-1}$, confirming that the initial decrease of surface area of CeO_2 occurs at the expense mostly of the micropores. It is worth noting that the subsequent reduction at 623 K does not modify the surface area of the CeO_2 sample but the microporosity is completely eliminated during this treatment. In agreement with the TPR profile of fresh CeO_2 reported in Fig. 3 and previous reports (4, 5) the reduction at 623 K should be limited only to the uppermost surface layers.

After a reduction at 780 K, which corresponds to the peak maximum in the trace 5 of Fig. 3, the surface area of CeO_2 decreases from 153 to 115 $m^2\ g^{-1}$. This is consistent with a recent observation that the reducing atmosphere promotes the CeO_2 sintering to a greater extent than the thermal treatment (38). Such a behaviour is attributed to an increased amount of oxygen vacancies under H_2 which can promote grain growth (39). In accord with this, in the

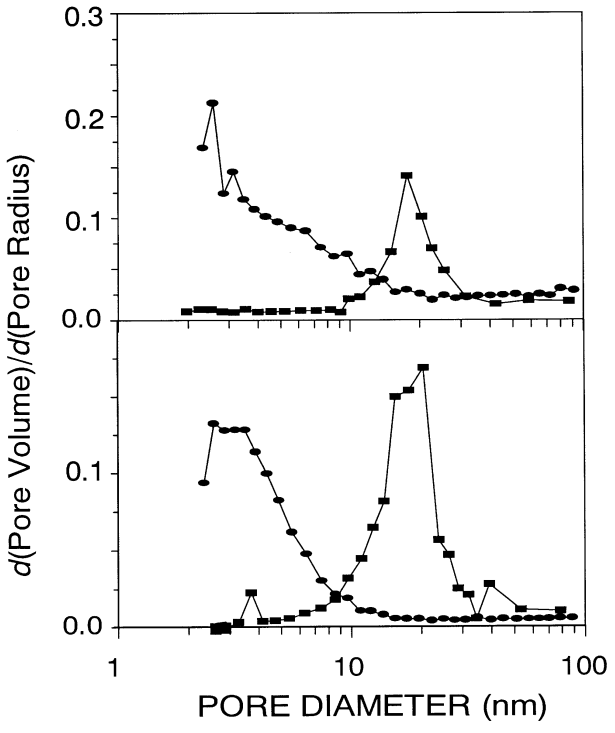

FIG. 5. Pore size distribution obtained from N_2 adsorption at 77 K over (1) fresh (•) and reduced 1073 K/oxidized 700 K (■) CeO_2 and (2) fresh (•) and reduced 1073 K/oxidized 700 K (■) $Ce_{0.5}Zr_{0.5}O_2$.

subsequent reductions carried out at 900 and 1000 K, the surface area of CeO_2 collapses to a final value of 11–12 m^2 g^{-1} (Table 4). Consideration of the TPR and OSC results clearly supports the idea that at moderate temperatures the redox capacity of CeO_2 is mainly controlled by the surface area. Moreover, they clearly indicate the critical importance of the stabilisation of surface area in the TWCs in order to avoid the deactivation of the catalysts.

Similarly, $Ce_{0.5}Zr_{0.5}O_2$ also reveals an enhanced sintering in the reducing conditions compared to a thermal treatment. There is, however, an interesting difference between the two systems: as shown by TPR of fresh $Ce_{0.5}Zr_{0.5}O_2$, the reduction starts at about 780 K, peaking at 900 K. The BET measurement shows that after the reduction at 780 K, the surface area strongly decreases. By contrast, the reduction of CeO_2 starts at about 623 K but no significant decrease of surface area is observed upon reduction at this temperature. Such an observation might be an indirect confirmation of the fact that in the $Ce_{0.5}Zr_{0.5}O_2$ the reduction occurs concurrently at the surface and in the bulk. Hence, a very strong decrease of the CeO_2 surface area occurs only at 900 K where the reduction in the bulk is attained.

Analysis of the isotherms carried out on the reduced/oxidized samples shows that the redox cycles strongly modify the texture of both the samples. The isotherms are still of type IV; however, both samples show hysteresis of type H3. This change is an indication of an extensive restructuring of the pores. Upon application of the Barret, Joyner, and Halenda (BJH) method (40) with the cylindrical pore size calculated from the Kelvin equation, mesopore distributions which are shown in Fig. 5 are obtained. For the fresh samples, a broad feature peaking below 4 nm is observed in both CeO_2 and $Ce_{0.5}Zr_{0.5}O_2$. This value corresponds to a p/p_o of 0.40 which suggests that the peak concerned has no real physical meaning and should be attributed to a tensile strength phenomenon (35). The presence of a contribution to the pore volume from micropores is confirmed by the V_t and V_{DR} reported in Table 4. These values suggest that most of the total pore volume reported in Table 4 has to be associated with pores whose diameters are below 10 nm.

Upon reduction/oxidation up to 1000 K, the initial pore structure is destroyed, the microporosity is no more detected, and formation of a new mesoporous structure with a unimodal distribution centred at 17–18 nm for both CeO_2 and $Ce_{0.5}Zr_{0.5}O_2$ is found. Note that despite the extensive sintering during these treatments, the cumulative pore volume is relatively unaffected in the $Ce_{0.5}Zr_{0.5}O_2$ and is comparable to that of sintered CeO_2 (Table 4).

The induction of a new mesoporosity in both CeO_2 and $Ce_{0.5}Zr_{0.5}O_2$ upon reduction/oxidation in the bulk is an important finding since it suggests that redox treatments can be easily employed to stabilise both the surface area and the pore structure against further sintering.

Scanning electron microscopy and powder XRD patterns. The SEM micrographs of fresh and recycled $Ce_{0.5}Zr_{0.5}O_2$ and CeO_2 are reported in Fig. 6. The fresh $Ce_{0.5}Zr_{0.5}O_2$ features the typical "mud-like" microstructure of a gel-derived product. Conversely, fresh CeO_2 shows the typical aspects of an agglomerated powder. Significantly, in spite of the different initial microstructure, the microstructure of both the recycled samples exhibits similar features with a discernible necking among the particles. The large surfaces are smoother in the case of $Ce_{0.5}Zr_{0.5}O_2$ than in the case of CeO_2, which is an indication that sintering has occurred to a larger extent in the former case.

In any case, both the samples conserve a large degree of porosity even after the redox cycles. It should be noted that in the case of the recycled $Ce_{0.5}Zr_{0.5}O_2$, there are grains which show a rather irregular surface (compare Fig. 6, picture 2, and the inset), suggesting that pores may have been formed in the treatment. Attribution of this pattern to a surface etching induced by the thermal treatments cannot be excluded. However, notwithstanding the limits of the spatial resolution of SEM, the inset of Fig. 6, picture 2, may suggest the presence of pores with a diameter $\leq$50 nm. This is in reasonable agreement with the pore distribution as determined from the N_2 adsorption isotherm at 77 K. It suggests that the appearance of the grain structure shown in picture 2 of Fig. 6 is best attributed to formation of mesoporosity which has been induced in both the samples by the redox cycles.

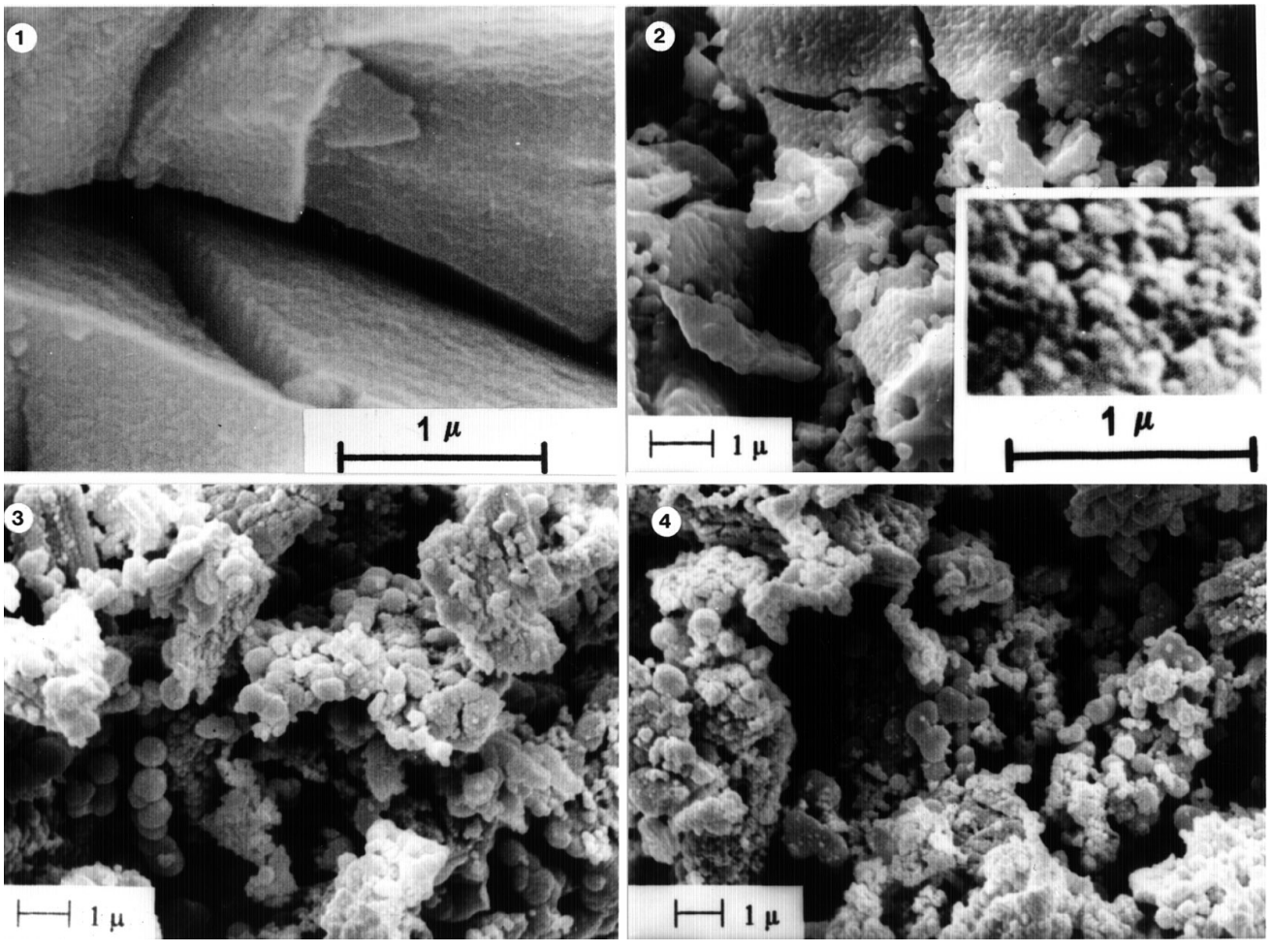

FIG. 6. SEM micrographs of (1) fresh, (2) threefold reduced/oxidized $Ce_{0.5}Zr_{0.5}O_2$ (in the inset the surface of the grains shown in the top part of Fig. 6.2 is magnified), and (3) fresh and (4) threefold recycled/oxidized CeO_2.

The formation of the mesoporosity should be attributed to stresses and to coalescence of dislocations induced by the large expansion/shrinkage of the lattice during the redox cycles. As shown in Fig. 1, after the reduction at 1273 K, the width of all the XRD peaks strongly decreases, which is an indication of an extensive sintering of the $Ce_{0.5}Zr_{0.5}O_2$. The average particle diameter calculated by the line broadening method increases from 5.4 to 68 nm. There is also a noticeable shift of all the peaks towards lower 2θ values, which corresponds to an expansion of about 1.0% of the cell parameter compared to the fresh sample. Upon reduction, the cerium ionic radius increases from 0.097 nm (Ce^{4+}) to 0.110 nm (Ce^{3+}). Upon reoxidation the cell parameter shrinks back to the initial value. The expansion/shrinkage is reversible and it could be reproduced in all the subsequent experiments. Also the XRD pattern of CeO_2 reveals an extensive sintering during the redox cycles (Fig. 1, trace 5); however, we could not detect the expansion/shrinkage of the cell parameter of the CeO_2 due to a fast reoxidation occurring at rt. An expansion of 2.8% was observed by Perrichon *et al.* upon reduction at 1073 K (2).

Summarising, the data reported in Table 4 and the micrographs shown in Fig. 6 indicate a parallel evolution of the microstructure both in $Ce_{0.5}.Zr_{0.5}O_2$ and in CeO_2, ruling out that textural modifications are responsible for the different reduction behaviour induced by the redox cycles in the mixed $Ce_{0.5}Zr_{0.5}O_2$ oxide compared to CeO_2.

An alternative explanation is therefore needed. As mentioned above, modification of surface properties could account for the variation of the initial temperature of the reduction of the $Ce_{0.5}Zr_{0.5}O_2$ surface; however, it cannot account for the strong decrease of the temperature of the reduction in the bulk upon sintering of the sample in the course of the TPR experiments. The behaviour is indeed quite singular. From the structural point of view, as shown in Fig. 1, trace 2, after the reduction at 1273 K, the resulting XRD pattern is still indexed in a Fm3m space group, indicating that the *cubic* structure is retained upon reduction. However, new peaks at 31.4°, 37.3°, and 44.9° (2θ), which

are indicated with an asterisk in Fig. 1 are observed in the XRD pattern. The integrated intensity of the reflection at 31.4° (2θ) is about 13% of the intensity of the (111) peak of the fluorite structure. These peaks are observed in all the subsequent spectra of both reduced and oxidized $Ce_{0.5}Zr_{0.5}O_2$. We were not able to attribute these peaks to any known CeO_2 or CeO_2–ZrO_2 phase. It should be noted that the CeO_2–ZrO_2 phase diagram is far from being completely understood and the presence of different phases was often inferred (11–17). Also for reduced CeO_2, a new cubic phase was recently reported (2).

The d spacing of the unknown phase changes in the redox cycles, suggesting that it contains a significant fraction of CeO_2. At 1273 K, significant reduction of ZrO_2 in the bulk is unlikely. Notably, the CeO_2 phase present in the fresh $Ce_{0.5}Zr_{0.5}O_2$ is no longer detected in both the reduced and oxidized form (Fig. 1, traces 2, 3). The lattice parameters of both the fresh and the reduced/oxidized $Ce_{0.5}Zr_{0.5}O_2$ are equal within experimental error, which suggests that the composition of the *cubic* phase is constant throughout the redox cycles. Consequently, the phase separation which occurs upon reduction to give rise to the unknown phase should be diffusionless in nature. This means that it should contain essentially pure CeO_2 even though reactions with interparticle amorphous ZrO_2 phase cannot be excluded. Such a reaction, of course, would generate a mixed CeO_2–ZrO_2 phase during the thermal treatment in H_2. Phase separation triggered by the Ce^{4+} reduction has been previously observed in *t*-$Ce_{0.12}Zr_{0.88}O_2$ (41, 42). Notably, this phase separation was observed above 1473 K where diffusional phase separation is likely to occur. Consistently, besides an unidentified phase, formation of $Ce_2Zr_2O_7$ was observed (41, 42). It should be noted that the low intensity of the peak at 31.4° (2θ) rules out a significant contribution of this phase to the redox behaviour of the system.

Raman spectroscopy. Figure 2, trace 2 reports the Raman spectrum of $Ce_{0.5}Zr_{0.5}O_2$ which has been reduced at 1000 K for 2 h and then reoxidized at 700 K. Comparison with data in Table 4 shows that such a treatment induces a strong sintering of the sample. The intensity of the T_{2g} mode at 465 cm^{-1} due to the symmetrical stretching of the oxygen around the central metal cation strongly decreases compared with the fresh sample which suggests that structural modification, not detectable by XRD, occurs. A band at 605 cm^{-1} is observed, suggesting that breaking of the selection rule due to some oxygen displacement from the ideal fluorite positions occurs with appearance of scattered phonons in the higher frequency tail.

The redox treatment up to 1273 K further modifies the Raman spectrum as shown by trace 3 of Fig. 2, which reports the spectrum of $Ce_{0.5}Zr_{0.5}O_2$ reduced at 1273 K and reoxidized at 700 K three times. The attributions of the peaks is very difficult due to the fact that, as reported above, during these cycles a small amount of a new phase was detected which could strongly affect the Raman spectrum. Notably, the T_{2g} mode at 465 cm^{-1} is no longer observed, suggesting that progressive displacement of the oxygen anions from their ideal position has occurred.

In the tetragonal phase a displacement of the oxygens alternatively upward and downward along the *z* axis was suggested (43). Such a displacement cannot be discerned in our case, since the position of the six bands of $A_{1g} + 3E_g + 2B_{1g}$ symmetry depends on the bond length and hence on the cerium content (21). Tetragonalization of the $Ce_{0.5}Zr_{0.5}O_2$ with sintering is consistent with the above observation that the phase stability and hence the stable/metastable phase diagram critically depends on the particle size.

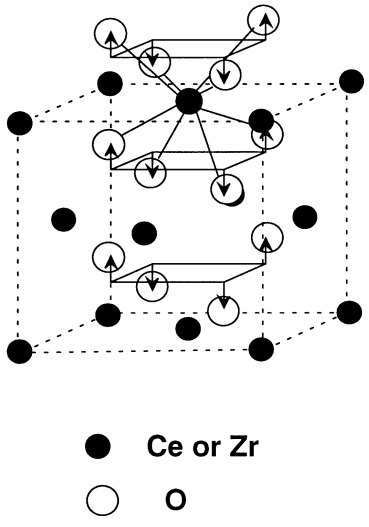

SCHEME 1

As shown above, the tetragonal distortion would alternatively shorten or elongate the metal–oxygen bonds. Moreover, the lengthening of the metal–oxygen bond will move the oxygen anions closer to the octahedral sites. Theoretical calculation showed that in the fluorite structure, the most energetically favourable path for the oxygen migration passes through the octahedral sites (44). Displacement of the oxygen anions toward the octahedral sites would therefore result in a lower energy barrier for the oxygen migration in the bulk, thus accounting for the promotion of the reduction in the bulk observed upon sintering of $Ce_{0.5}Zr_{0.5}O_2$. consistently, for this process, the oxygen migration was suggested to be rate limiting (6).

CONCLUSIONS

The results show that the TPR behaviour of the fresh $Ce_{0.5}Zr_{0.5}O_2$ depends on its initial microstructure. High surface area favours reduction at lower temperatures compared to an extensively sintered sample ($\approx$1 $m^2\ g^{-1}$). This behaviour appears to be consistent with that of CeO_2. The reduction/oxidation processes strongly modify the

microstructure of the two samples: in both cases the reduction up to 1000–1273 K decreases the surface area to approximately 10 $m^2\ g^{-1}$; however, the occurrence of the redox process in the bulk induces formation of mesoporosity which prevents further sintering.

The comparison of the redox behaviour of CeO_2 with the structurally doped $Ce_{0.5}Zr_{0.5}O_2$ shows that at moderate temperatures the redox processes are strictly surface-related in the former case. At variance with this, in $Ce_{0.5}Zr_{0.5}O_2$ the redox behaviour is strongly modified since the reduction occurs concurrently at the surface and in the bulk of the solid solution. Furthermore, the structural modifications induced by the substitution of Ce^{4+} by Zr^{4+} appear to be responsible for the unusual enhancement of the reduction processes observed in the sintered $Ce_{0.5}Zr_{0.5}O_2$ compared with the high surface area sample.

The availability of bulk Ce(IV) sites for the redox processes at moderate temperatures, even after extensive sintering, makes these materials highly attractive for any industrial process which requires a highly efficient redox couple with a high thermal stability.

ACKNOWLEDGMENTS

Dr. L. Murrel is gratefully acknowledged for giving us the CeO_2 sample. An anonymous referee is acknowledged for helpful suggestions concerning the textural properties. CNR and MURST 40% (Roma), Università di Trieste and Magneti Marelli D.S.S. (Torino) are acknowledged for financial support.

REFERENCES

1. Taylor, K. C., *in* "Catalysis—Science and Technology" (J. R. Anderson and M. Boudart, Eds.), Vol. 5. Springer-Verlag, Berlin, 1984. *Catal. Rev.-Sci. Eng.* **35**, 457 (1993).
2. Perrichon, V., Laachir, A., Bergeret, G., Fréty, R., Tournayan, L., and Tóuret, O., *J. Chem. Soc. Faraday Trans.* **90**, 773 (1994).
3. Yao, H. C., and Yu Yao, Y. F., *J. Catal.* **86**, 254 (1984); Harrison, B., Diwell, A. F., and Hallett, C., *Platinum Met. Rev.* **32**, 73 (1988).
4. Laachir, A., Perrichon, V., Badri, A., Lamotte, J., Catherine, E., Lavalley, J. C., El Fallah, J., Hilaire, L., Le Normand, F., Quemere, E., Sauvion, N. S., and Touret, O., *J. Chem. Soc. Faraday Trans.* **87**, 1601 (1991).
5. El Fallah, J., Boujana, S., Dexpert, H., Kiennemann, A., Majerus, J., Touret, O., Villain, F., and Le Normand, F., *J. Phys. Chem.* **98**, 5522 (1994).
6. Ranga Rao, G., Kašpar, J., Meriani, S., Di Monte, R., and Graziani, M., *Catal. Lett.* **24**, 107 (1994); Fornasiero, P., Di Monte, R., Ranga Rao, G., Kašpar, J., Meriani, S., Trovarelli, A., and Graziani, M., *J. Catal.* **151**, 168 (1994).
7. Courty, P., and Marcilly, C., *in* "Preparation of Catalysts" (B. Delmon, P. A. Jacobs, and G. Poncelet, Eds.), p. 119. Elsevier, Amsterdam, 1976.
8. Balducci, G., Fornasiero, P., Di Monte, R., Kašpar, J., Meriani, S., and Graziani, M., *Catal. Lett.* **33**, 193 (1995).
9. Meriani, S., and Soraru, G., "Ceramic Powders" (P. Vicenzini, Ed.), p. 547. Elsevier, Amsterdam, The Netherlands, 1983.
10. Malet, P., and Caballero, A., *J. Chem. Soc. Faraday Trans. I* **84**, 2369 (1988); Monti, D. A. M., and Baiker, A., *J. Catal.* **83**, 323 (1983).
11. Tani, E., Yoshimura, M., and Somiya, S., *J. Am. Ceram. Soc.* **66**, 506 (1983).
12. Duran, P., Gonzalez, M., Moure, C., Jurdo, J. R., and Pascal, C., *J. Mater. Sci.* **25**, 5001 (1990).
13. Yashima, M., Morimoto, K., Ishizawa, N., and Yoshimura, M., *J. Am. Ceram. Soc.* **76**, 1745 (1993).
14. Meriani, S., *Mater. Sci. Eng.* **A109**, 121 (1989).
15. Yashima, M., Morimoto, K., Ishizawa, N., and Yoshimura, M., *J. Am. Ceram. Soc.* **76**, 2865 (1993).
16. Yashima, M., Arashi, H., Kakihana, M., and Yoshimura, M., *J. Am. Ceram. Soc.* **77**, 1067 (1994).
17. Meriani, S., *Mat. Sci. Eng.* **71**, 369 (1985); Meriani, S., and Spinolo, G., *Powder Diffr.* **2**, 255 (1987).
18. Keramidis, V. G., and White, W. B., *J. Am. Ceram. Soc.* **57**, 22 (1974).
19. McBride, J. R., Hass, K. C., Pindexter, B. D., and Weber, W. H., *J. Appl. Phys.* **76**, 2435 (1994).
20. Pal'guev, S. F., Alyamosvkii, S. I., and Volchenkova, Z. S., *Russ. J. Inorg. Chem.* **4**, 1185 (1959).
21. Kim, D., Jung, H., and Yang, I., *J. Am. Ceram. Soc.* **76**, 2106 (1993).
22. Garvie, R. C., *J. Phys. Chem.* **69**, 1238 (1965); **82**, 218 (1978); Garvie, R. C., and Goss, M. F., *J. Mater. Sci.* **21**, 1253 (1986).
23. Mitsuhasi, T., Ichihara, M., and Tatsuke, U., *J. Am. Ceram. Soc.* **57**, 97 (1974).
24. Livage, J., Doi, K., and Mazières, C., *J. Am. Ceram. Soc.* **51**, 349 (1968).
25. Tani, K., Yoshimura, M., and Somiya, S., *J. Am. Ceram. Soc.* **66**, 11 (1983).
26. Yoldas, B. E., *J. Am. Ceram. Soc.* **65**, 387 (1982); Chatterjee, A., Pradhan, S. K., De Datta, A. M., and Chakravorty, D., *J. Mater. Res.* **9**, 263 (1994).
27. Zotin, F. M. Z., Tournayan, L., Vardloud, J., Perrichon, V., and Fréty, R., *Appl. Catal. A* **98**, 99 (1993).
28. Fierro, J. L. G., Soria, J., Sanz, J., and Rojo, J. M., *J. Solid State Chem.* **66**, 154 (1987).
29. Fierro, G., Lo Jacono, M., Inversi, M., Porta, P., Lavecchia, R., and Cioci, F., *J. Catal.* **148**, 709 (1994).
30. Killner, J. A., and Steela, B. C. H., *in* "Non-Stoichiometric Oxides" (O. T. Sorensen, Ed.), Chap. 5. Academic Press, New York, 1981.
31. Kundo, J., Abe, H., Sakata, Y., Maruya, K., Domen, K., and Onishi, T., *J. Chem. Soc. Faraday Trans. I* **84**, 511 (1988).
32. Bolis, V., Morterra, C., Volante, M., Orio, L., and Fubini, B., *Langmuir* **6**, 695 (1990).
33. Bosman, H. J. M., Kruissink, E. C., van der Spoel, J., and van den Brink, F., *J. Catal.* **148**, 660 (1994).
34. Sing, K. S. W., Everett, D. H., Haul, R. A. W., Moscou, L., Pierotti, R. A., Rouquérol, J., and Sieminiewska, T., *Pure Appl. Chem.* **57**, 603 (1985).
35. Gregg, S. J., and Sing, K. S. W., "Adsorption, Surface Area and Porosity." Academic Press, New York, 1982.
36. Harkins, W. D., and Jura, G., *J. Chem. Phys.* **11**, 430 (1943).
37. Lecloux, A. J., *in* "Catalysis, Science and Technology" (J. R. Anderson and M. Boudart, Eds.), Vol. 2, Chap. 4. Springer-Verlag, Berlin, Germany, 1981.
38. Perrichon, A., Laachir, A., Abouarnadasse, S., Touret, O., and Blanchard, G., *Appl. Catal. A* **129**, 69 (1995).
39. Kingery, W. D., Bowen, H. K., and Uhlmann, D. R., "Introduction to Ceramics," 2nd ed., Chap. 10. Wiley, New York, 1976.
40. Barret, E. P., Joyner, L. G., and Halenda, P. P., *J. Am. Chem. Soc.* **73**, 373 (1951).
41. Heussner, K. H., and Claussen, N., *J. Am. Ceram. Soc.* **72**, 1044 (1989).
42. Zhy, H., Hirata, T., and Muramatsu, Y., *J. Am. Ceram. Soc.* **75**, 2843 (1992).
43. Yashima, M., Ishizawa, N., and Yoshimura, M., *J. Am. Ceram. Soc.* **75**, 1550 (1992).
44. Hagenmuller, P., "Solid Electrolytes, General Principles, Characterization, Material, Applications," Material Science Series, W. Vangool, 1978.